SAND2015-5214C

Development of a RANS and LES/RANS Flow Solver for High-Speed Engine Flowpath Simulations

Jack R. Edwards[1]
North Carolina State University, Raleigh, North Carolina

Jesse A. Fulton[2]
Sandia National Laboratories, Albuquerque, NM

The development of a reactive flow solver suitable for large-scale simulations of high-speed engine component flow fields is described in this paper. The intent is to mature an existing flow solver, North Carolina State University's REACTMB, into a production-level tool suitable for test and evaluation (T&E) activities. The computational framework is based on the combined use of Reynolds-averaged Navier-Stokes (RANS) methods and large-eddy simulation (LES) strategies, with the former used to examine system-level effects and the latter used for detailed component studies. Specific modifications that extend the capabilities of REACTMB (bleed modeling, eddy-dissipation combustion modeling) are described, as are methods for coupling flow solutions with established 1D system performance tools.

1. Introduction

Analysis tools for testing and evaluation (T&E) of high-speed flight vehicles range generally from system-level (usually quasi-1D) models for component performance to medium-fidelity techniques (Reynolds-averaged Navier-Stokes (RANS) flow solvers) to high-fidelity techniques based on large-eddy simulation (LES) that can be used for detailed component simulations. It is essential that the strategies used are compatible with one another and that appropriate exchanges of information among the tools takes place in a manner consistent with the analyzer's requirements. This article describes the development of a RANS/LES flow solver that is specifically designed for T&E purposes. The solver is based on North Carolina State University's established REACTMB platform [1-5], which has been used most recently to conduct large-eddy simulations of scramjet combustor flowfields. The general capabilities of REACTMB are described, as are new additions that improve the utility of REACTMB for general T&E applications. These include boundary-layer bleed models, eddy-dissipation combustion models for rapid analyses of heat release effects, and modules for determining stream-thrust-averaged 1D quantities for coupling Navier-Stokes solutions with established system-level performance tools. Several examples of current capabilities are described to conclude the paper.

---

[1] Professor, Department of Mechanical and Aerospace Engineering, Associate Fellow, AIAA.
[2] Senior Member of Technical Staff, Member, AIAA.

Sandia National Laboratories is a multi-program laboratory managed and operated by Sandia Corporation, a wholly owned subsidiary of Lockheed Martin
Corporation, for the U.S. Department of Energy's National Nuclear Security Administration under Contract DE-AC04-94AL85000.

2. REACTMB

REACTMB solves the compressible Navier-Stokes equations for a mixture of gases in thermal equilibrium and chemical non-equilibrium on general, multi-block structured meshes using a finite-volume method. Gridgen and GridPro mesh-generation techniques are usually employed, but the multi-block meshes generated are often sub-divided into even smaller blocks to facilitate load-balancing. MPI message-passing techniques are used to transfer information among processors. The discretization of the inviscid fluxes utilizes the Low Diffusion Flux-Splitting Scheme (LDFSS) [6], an approximate Riemann solver developed from 1995-1997 as an improvement to Liou's AUSM flux-splitting method [7]. Implicit methods are used for time advancement, with sub-cycling strategies used to maintain time accuracy if required. A Crank-Nicholson discretization of the Navier-Stokes system at a specific time level reads as follows:

$$solve:\left[\Omega M(\frac{1}{\Delta t}+\frac{1}{\Delta \tau})+A\right]^{n}\Delta V^{n+1,k+1}=-\left(\Omega\frac{U^{n+1,k}-U^{n}}{\Delta t}+\frac{1}{2}[R(U^{n+1,k})+R(U^{n})]\right) \quad (1)$$

Here, Ω is the cell volume, U is the vector of conservative variables, V is a vector of primitive variables ($V=[\rho_1,\ldots,\rho_N,u,v,w,T,k,\omega]^T$), and R is the Navier-Stokes residual vector, which includes source terms for chemical reaction. The linear system formed at each sub-iteration is solved approximately using an incomplete LU decomposition method. Optionally, the solution of the linear system itself can be iteratively improved via another sub-iteration procedure. This step involves message-passing of solution corrections between mesh blocks, thus serving as a means of ensuring a tighter coupling among equations. The user has the option of freezing the evaluation and factorization of the matrix elements either over the course of the sub-cycles (the usual practice) or over several physical time steps. The user may also invoke a 'storage efficient' option which only allocates storage sufficient for the largest block mapped to a particular processor. Other blocks on the same processor use the same storage space, meaning that the option for iterative improvement is disabled and no freezing of matrix elements can take place. This option is often used for RANS applications that seek a steady state.

The T&E version of REACTMB contains two methods for extending the baseline first-order LDFSS flux formulation to a higher spatial order of accuracy. The first is based on total variation diminishing (TVD) limiting strategies, applied to the variable vector $W=[p_1,\ldots,p_N,u,v,w,T,k,\omega]^T$ and the second is based on the Piecewise Parabolic Method (PPM). TVD methods are usually used for RANS applications, while PPM is usually used for LES by virtue of its lower level of dissipation. Both can be utilized with the 'Ducros switch' [8], which shifts the interpolations from TVD / PPM to fourth-order central differences in regions where the vorticity greatly exceeds the velocity divergence. This is commonly used in LES applications.

3. Turbulence Modeling

Turbulence modeling within the T&E version of REACTMB is based on the Menter BSL/SST k-ω model. [9] An option to utilize LES/RANS hybridization strategies developed at NCSU [10] to shift the closure to LES away from solid surfaces is also present. Hybridization is accomplished by defining the eddy viscosity as follows

$$\mu_t = \rho\left[(1-\Gamma)\nu_{t,sgs} + \Gamma\frac{k}{\omega}\right], \tag{2}$$

where Γ is a blending function that connects the RANS and LES branches. A mixed-scale algebraic model due to Lenormand, et al. [11] has been used for the subgrid-scale eddy viscosity in all recent applications. The blending function is defined as

$$\Gamma = \frac{1}{2}[1-\tanh(\beta(\frac{1}{\lambda^2}-1))] \tag{3}$$

with λ being a ratio of inner and outer turbulence length scales:

$$\lambda = g(\Delta_{\max}, l_{outer})\frac{l_{outer}}{l_{inner}},\ l_{inner} = \kappa d,\ l_{outer} = \alpha\sqrt{\frac{10\nu\langle\omega\rangle + \langle k\rangle + \langle k_R\rangle}{C_\mu^{1/2}\langle\omega\rangle\omega}} \tag{4}$$

Here, $\langle k_R\rangle = \frac{1}{\langle\rho\rangle}\frac{1}{2}(\langle\rho u_k u_k\rangle - \frac{\langle\rho u_k\rangle\langle\rho u_k\rangle}{\langle\rho\rangle})$ is the resolved turbulence kinetic energy, and the brackets represent the use of exponentially-weighted time averages of the resolved fields (this provides the 'ensemble average'). The model constants α and β are currently assigned values of 1.5 and 15 [10]. As the model is dependent on both inner-layer and outer-layer length-scale information, it is capable of adjusting to strong departures from local equilibrium and can respond to large changes in boundary-layer thickness without problem-specific adjustment.

The mesh-scale dependent parameter $g(\Delta_{\max}, l_{outer})$ is a recent addition to the model [12], motivated by the need to recover a RANS closure for meshes in which the wall-parallel spacing is not sufficient to resolve an outer-layer length scale:

$$g(\Delta_{\max}, l_{outer}) = \min[10, \max(1, \frac{1}{2}\frac{\Delta_{\max}}{l_{outer}})],\quad \Delta_{\max} = \max(\Delta_x, \Delta_y, \Delta_z) \tag{5}$$

The mesh-scale dependent component is not active if the boundary layers are well resolved in all directions. This version of the model has been used to predict heating loads on the afterbody of a scale model of NASA's Orion re-entry capsule [12] and in simulations pre-mixed flame propagation in a dual mode combustor [13].

4. Reaction Chemistry Modeling

The T&E version of REACTMB includes several techniques for modeling hydrogen and hydrocarbon combustion chemistry. Finite-rate chemical reaction models based on the law of mass action can be invoked for hydrogen-air combustion and ethylene-air combustion [14-16], while quasi-global models are in place for JP-7 combustion [17]. Source terms determined by automatic reaction-reduction techniques are available for ethylene / methane mixtures. [18] As any finite-rate treatment of chemical kinetics incurs additional expense associated with the need to track different chemical components, simpler approaches based on Magnussen's eddy dissipation concept (EDC) [19] have been incorporated into the T&E version for RANS-based applications. One-, two, and three-step mechanisms can be invoked using EDC for general hydrocarbons. In EDC, the reaction rate is proportional to a turbulent time scale determined from the Menter k-ω model. Given a reaction of the form $\nu_A A + \nu_B B \Rightarrow \nu_C C + \nu_D D$, the EDC

prescription of the production rate for species C (for example) would be

$$\dot{\omega}_C = A_{EDC}\beta^*\omega\nu_c \min\left(\frac{\rho_A}{\nu_A M_{w,A}}, \frac{\rho_B}{\nu_B M_{w,B}}\right), \quad T > T_{ign} \qquad (6)$$

$$\dot{\omega}_C = 0, \quad T < T_{ign}$$

where T_{ign} is a user-specified 'ignition temperature' (~900 K for hydrogen and ethylene combustion) and A_{EDC} is a model constant, usually selected to be between 1 and 4. EDC reactions are allowed to proceed only in the forward direction. Turbulence / chemistry interactions are not explicitly accounted for in the finite-rate RANS models; however, simple strategies based on the assumption of a partially-stirred reactor can be invoked for the LES models. [20, 21] These scale the source terms by the ratio of a subgrid-scale mixing time scale to a characteristic chemical reaction time scale.

5. Bleed Modeling

High speed inlets often require the use of boundary layer bleed to stabilize shock waves and to reduce blockage caused by shock / boundary layer interactions. While direct simulation of flow through bleed passages is possible [22, 23], it requires extensive mesh resolution and knowledge of plenum geometries, plenum pressures, and exiting mass flow rates for each part of the bleed system. A more cost-effective approach is to model the effects of bleed plates. In REACTMB, we adopt two strategies for accomplishing this. The first simply imposes the bleed mass flow rate (including porosity effects) over a user-specified section of a solid surface. The second is a simplified version of an approach presented by Slater [24] in which a quasi-1D formulation of the flow through a bleed hole is combined with experimentally-determined discharge coefficients to yield an approach that can predict the 1D mass flux and can account for the effects of external interactions, such as shock impingement onto the bleed plate. The specific formulation follows that of Baurle and Norris [23]. First, a sonic flow coefficient is computed based on the ratio of wall to plenum pressures as follows:

$$Q^*_{sonic} = 0.59799735 + 0.03069346\left(\frac{p_{plenum}}{p_{wall}}\right) - 0.59361420\left(\frac{p_{plenum}}{p_{wall}}\right)^2 \qquad (7)$$

Then, a reference sonic mass flow rate is calculated for each surface cell in the bleed region:

$$\dot{m}_{sonic} = p_{wall}\phi A_{cell}\left(\frac{\gamma}{RT_w}\right)^{1/2}\left(\frac{\gamma+1}{2}\right)^{\frac{\gamma+1}{2(1-\gamma)}} \qquad (8)$$

The actual mass flow rate is then defined as $\dot{m}_{bleed} = \dot{m}_{sonic}Q^*_{sonic}$. To complete the description of the flow properties within the bleed region, one must first solve for the average Mach number of the flow within a bleed hole:

$$\dot{m}_{bleed} = p_o\phi A_{cell}M_{hole}\left(\frac{\gamma}{RT_o}\right)^{1/2}\left(1+\frac{\gamma-1}{2}M^2_{hole}\right)^{\frac{\gamma+1}{2(1-\gamma)}},$$

$$p_o = p_{wall}, \quad T_o = T_{wall} \qquad (Q^*_{sonic} \geq 0) \qquad (9)$$

$$p_o = p_{plenum}, \quad T_o = T_{plenum} \qquad (Q^*_{sonic} < 0)$$

From this, one can get the pressure and temperature within the hole,

$$T_{hole} = T_o / (1 + \frac{\gamma - 1}{2} M_{hole}^2)$$
$$p_{hole} = p_o (T_{hole} / T_o)^{\gamma/(\gamma-1)} \quad (10)$$

the velocity component normal to the surface $\vec{V} \cdot \vec{n} = M_{hole} \sqrt{\gamma R T_{hole}}$, and the components of the surface velocity $\vec{V} = (\vec{V} \cdot \vec{n})\vec{n}$. Dependent variables such as the enthalpy can be calculated at the surface, based on this information. The present implementation differs from [23, 24] in that no provision is made to adjust the plenum pressure so that a target bleed mass flow rate is achieved.

6. Performance Measures

As a primary use of the T&E version of REACTMB is to support ground and flight tests of hypersonic vehicles, standard measures of performance (forces, moments, integrated heating load, surface shear stress, combustion efficiency, mixing efficiency) have been added as post-processing output. In addition, strategies for performing stream-thrust averaging on general multi-block meshes have been incorporated, following [25]. (In [25], this particular procedure is referred to as CMME averaging.) The method employed for stream-thrust averaging performs the following steps.

1. First, a set of planes perpendicular to the nominal streamwise direction is defined. Information from this step includes the location of one point within the plane and the outward normal to the plane.
2. Then, a pre-processing routine searches the computational mesh and identifies the mesh blocks that the planes are located within as well as the mesh coordinate plane that is closest to the plane in question. Output from the pre-processor includes the coordinate direction that nearest to being perpendicular to the plane, and the coordinate of the nearest plane in that direction. This is done for every block in the mesh; if a block does not contain the plane of interest, the coordinate direction is assigned to be zero. A weighting parameter is also extracted – this is used to average results from the nearest plane and its immediate neighbor in the frequent case that the actual plane lies between two mesh-coordinate planes. This information is written out to a file for REACTMB to read.
3. Based on the above input, REACTMB then calculates mass, momentum, energy, species, and turbulence kinetic-energy fluxes, along with estimates of the product of the average pressure and the plane area and the average plane normal, for each mesh block that contains each streamwise plane. These values are then summed to a root processor using MPI_REDUCE commands and are organized according to the streamwise plane.
4. Next, stream-averaged values for the total enthalpy along with the state equation are used to solve for the actual product of average pressure and area using a bisection / Newton method. If no solution exists, then a global minimum solution is sought. This formulation is similar to that described in [25] but solves for pressure instead of temperature, thus eliminating an inner iteration.
5. The final step then decodes stream-thrust averaged velocity components, density, temperature, pressure, mass fraction, and Mach number.

7. Results

The T&E version of REACTMB is undergoing beta-testing. Some results have been obtained as discussed in the following subsections.

7.1. EDC combustion modeling: hydrogen-air mixtures

Figure 1 shows centerplane temperature contours in the combustor section of a model scramjet tested in GASL's Hypulse facility. The three-dimensional mesh contains ~11 M cells and includes inlet, isolator, combustor, and nozzle sections. Previous simulations of this case were conducted using a hydrogen-silane mixture, as experimental results failed to show ignition at a Mach 7 flight enthalpy condition. [26] Results from the EDC combustion model and a 9-

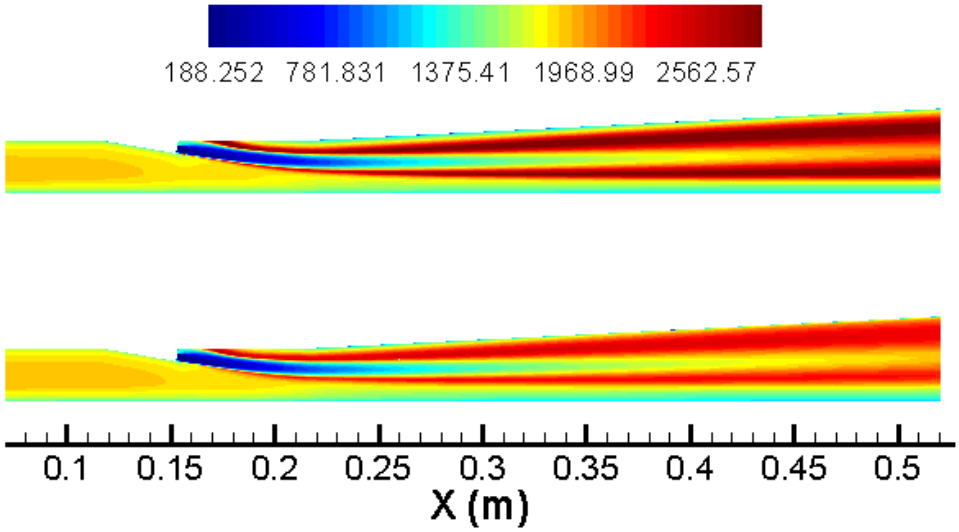

Figure 1: Centerplane temperature comparisons (top, Eddy Dissipation Concept; bottom, 9-species finite-rate)

species finite-rate hydrogen-air reaction model [15] are compared in the figure. In this case, the free-stream temperature is raised to 1200 K and the free-stream Mach number is set at 2.2 to ensure dual-mode (subsonic) combustion and auto-ignition with the finite-rate model without silane. The predictions are very close in terms of flame structure (and overall heat release) but as expected, the single-step EDC model yields higher peak flame temperatures.

7.2. EDC combustion modeling: ethylene-air mixtures

Simulations have also been conducted for cavity-stabilized ethylene combustion in a direct-connect axisymmetric dual-mode combustor at the Air Force Research Laboratories' Research Cell 22. [27]. In this case, ethylene reaction was modeled using a seven-species, three-step EDC formulation in order to help reduce computation time to a level more suitable for T&E activities. The use of such a model requires some additional overhead time in the form of a case-specific calibration of quantities such as EDC reaction rate coefficient (A_{EDC}) and turbulent Schmidt number, Sc_t. The results of this calibration are given in Figures 2 and 3, which plot experimental wall pressure data along with computed wall pressures for a low and a high equivalence ratio. In addition, one-dimensional pressures from REACTMB's stream-thrust-averaging computation are

also shown, and a radial slice contour plot of Mach number is located at the bottom of each figure, scaled to fit the horizontal axis of the pressure plots. (The lower boundary of the contour plot is the combustor centerline.)

Figure 2 shows the operation of the combustor at a low equivalence ratio of $\Phi = 0.30$. Fuel injection takes place just upstream of the annular cavity, within which the flame appears well-stabilized. An initial precombustion shock is located just upstream of the injection location, causing an initial combustor pressure rise that compresses the core flow and aids combustion. Mach numbers are lowest in this region of the combustor, but are still largely greater than unity and so the combustor is operating in scram mode. Further downstream, an abrupt area step in the combustor results in sudden expansion of the core flow and an additional recirculation region just behind the step that results in a secondary region of flame stabilization. Here the Mach number is much higher and there are multiple shock reflections as the flow travels toward the end of the combustor.

The level of agreement in wall pressure distribution between experiment and computation is quite good. These results indicate that it is possible to use EDC reactive chemistry without sacrificing predictive capability, provided that a careful calibration is first carried out. (Initial simulations before calibration resulted in wall pressure distributions that were in poor agreement with experiment.) In addition, the one-dimensional pressure data (blue squares) follow the general trend of the wall pressure distribution rather well. The only exception to this is a point located at $x = 1.1$ m, where the stream thrust averaged pressure seems abnormally low. This is due to the high amount of flow distortion at this point in the combustor, where heat is being released and shocks are being generated. The particular averaging method used in this work (the CMME method) tends to have more difficulty in regions of high flow distortion and this limitation needs to be taken into account when these types of studies are performed. In addition, this point happens to be located where the core flow (away from the wall) contains an expansion as part of the supersonic combustor shock/expansion structure. The wall pressure at this location therefore will be higher than the pressure in the core region, and so the stream-thrust-averaged pressure will be lower than the pressure at the wall as well.

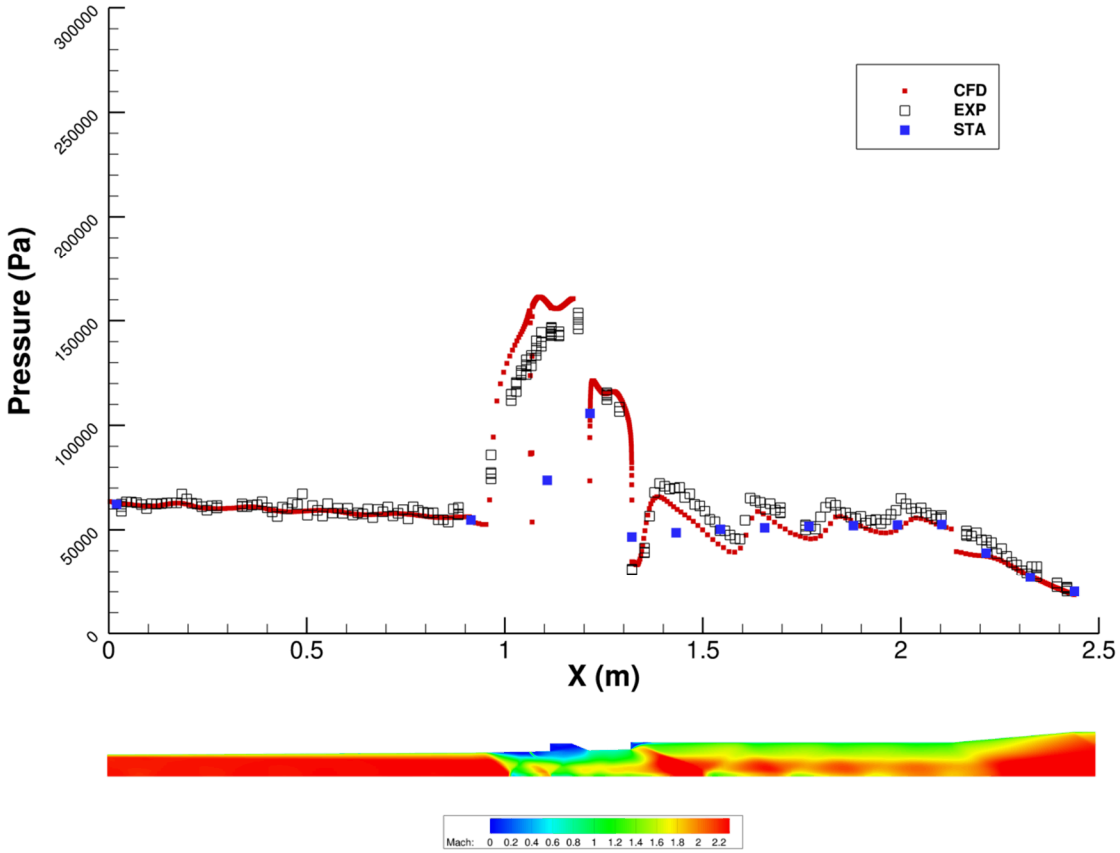

Figure 2. Mach contours and wall pressure distribution in AFRL RC22 combustor during Φ = 0.30 operation.

Mode transition behavior is an especially difficult issue to handle in CFD simulations of high-speed propulsion systems. This is because of the complex interactions between reactive chemistry, boundary layers, and shock structures that function as the fundamental mechanism of mode transition. Figure 3 shows pressure and Mach contour data for the RC22 combustor at a relatively high equivalence ratio of Φ = 0.89. At this fuel setting, combustor pressures have risen to the point at which the shock structures in the combustor have traveled upstream into the isolator region and stabilized there. It can be seen that the predicted shock train position matches the experimental measurements very closely. Peak combustor pressures are also well-predicted using REACTMB. This further indicates that the EDC model methodology is sufficient to properly capture combustor mode transition after calibration. In addition, the stream-thrust-averaged combustor pressures match CFD and experiment rather well.

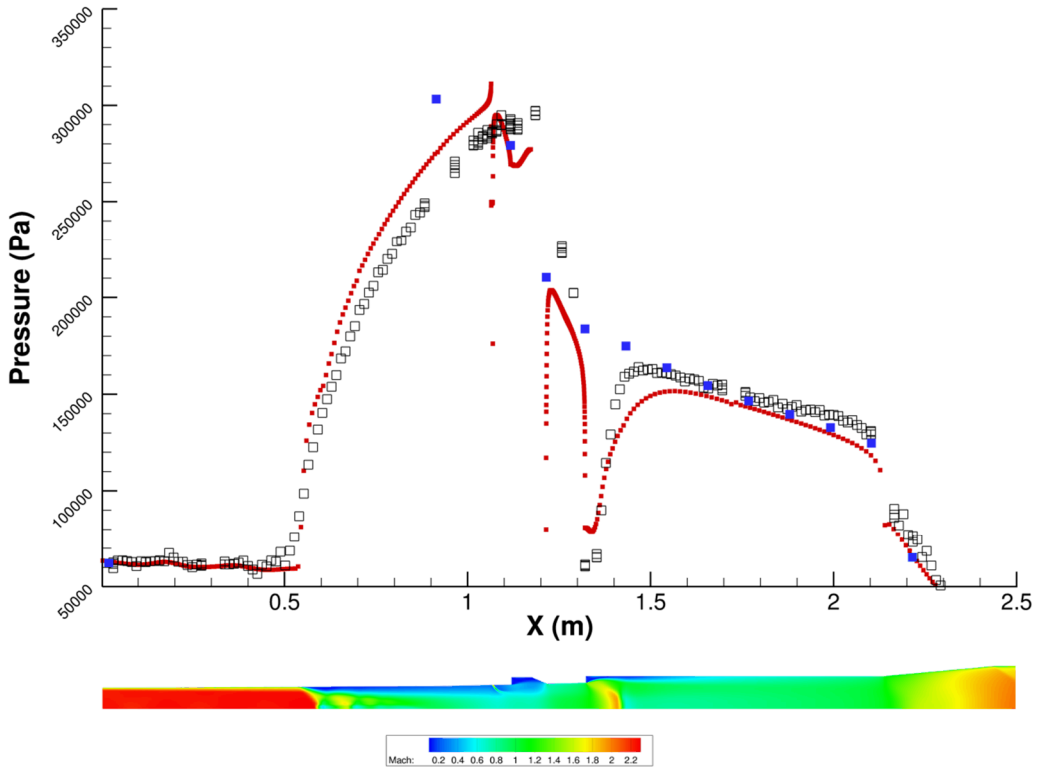

Figure 3. Mach contours and wall pressure distribution in AFRL RC22 combustor during Φ = 0.89 operation.

7.3. Comparison with SRGULL

Figure 4 shows a two-dimensional mesh generated to compare REACTMB results with NASA's SRGULL one-dimensional scramjet engine analysis code [28]

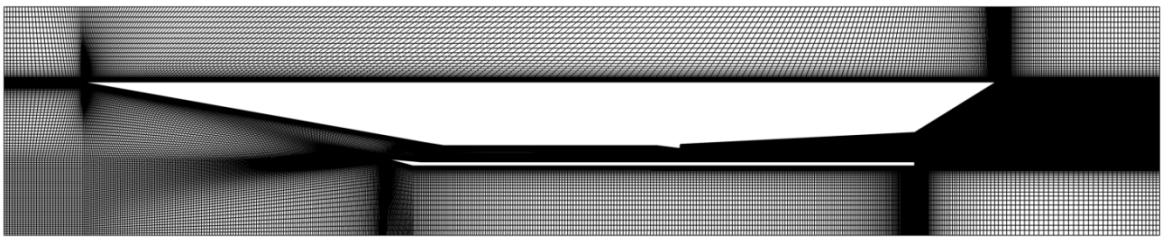

Figure 4: 2D scramjet flowpath mesh

Free-stream conditions are set for flight at Mach 7 at a dynamic pressure of 1000 psf. The wall temperature is set at 600 K. The EDC model for hydrogen-air combustion is used. Results have been obtained for a mixing-only case and a combusting case at an equivalence ratio of 0.5.

SRGULL is a compilation of various legacy NASA codes into a unified program specially intended for ramjet and scramjet simulations. At its core is a one-dimensional combustor code that is capable of ramjet, scramjet, and dual-mode propulsion-system simulations. SRGULL requires geometry input for the entire flowpath from inlet to nozzle. It then executes a two-dimensional Euler simulation of the inlet flowfield and uses the results to run a boundary-layer solution along the inlet walls. The 2-D inlet solution is then stream-thrust averaged at the inlet throat and modified to account for viscous losses, after which the information is passed to the one-dimensional combustor code. The combustor code takes input regarding fuel flow rate, heat release schedule, and many other parameters, and predicts one-dimensional flow properties along the combustor length. It can also produce upper and lower surface-property data. Flow data at the combustor exit is used to initialize the nozzle solution, which is executed in the same way as the inlet solution. Table 1 presents comparisons between SRGULL and REACTMB for performance parameters and for cross-sectional averages for the mixing-only case. REACTMB results are stream-thrust averaged at several stations to enable comparisons with SRGULL.

Table 1: REACTMB / SRGULL Comparisons: Mixing

Cowl-To-Tail Data				
		REACTMB	SRGULL	% Error
Fx	N	-137.46	-136.6	0.63
Fy	N	-92.29	-89.63	2.88
Mz	N-m	-85.75	-101.75	-18.66

Nose-To-Tail Data				
		REACTMB	SRGULL	% Error
Thrust	N	110.5	109.7	0.72
Isp	s	122.5	121.5	-0.82

Inlet Throat Data				
		REACTMB	SRGULL	% Error
Mach		4.09	4.09	0.0
Static Press	Pa	12024	11955	-0.57
1D Vel (vdotn)	m/s	1911	1912	0.05
x-ST	N	278.8	279	0.07
y-ST	N	-16.04	-16.05	-0.31
Dynamic Pressure	Pa	138555	138127	-0.31
Static Temp	K	552	549	-0.54
Static Dens	kg/m^3	0.0756	0.0756	0.0
Mass Flow	kg/s	0.1398	0.1399	0.07

Combustor Exit Data				
		REACTMB	SRGULL	% Error
Mach		2.94	3.31	12.59
Static Press	Pa	18524	15073	-18.63
1D Vel (vdotn)	m/s	1655	1718	3.81
x-ST	N	414.3	424.3	2.41
y-ST	N	5.46	10.07	84.43
Dynamic Pressure	Pa	109473	114069	4.20
Static Temp	K	715	601	-15.94
Static Dens	kg/m^3	0.0799	0.0773	-3.25
Mass Flow	kg/s	0.225	0.232	3.11

Body-side and cowl-side wall pressure distributions are given in Figure 5. The results show that SRGULL is capable of capturing the general responses but cannot reproduce pressure oscillations that occur from shock reflections in the combustor. The exit flow from the combustor is predicted to be faster in SRGULL, presumably due to its inability to capture losses due to shock systems. Despite these differences, the axial and normal forces, thrust and specific impulse predicted by SRGULL agree with REACTMB remarkably well.

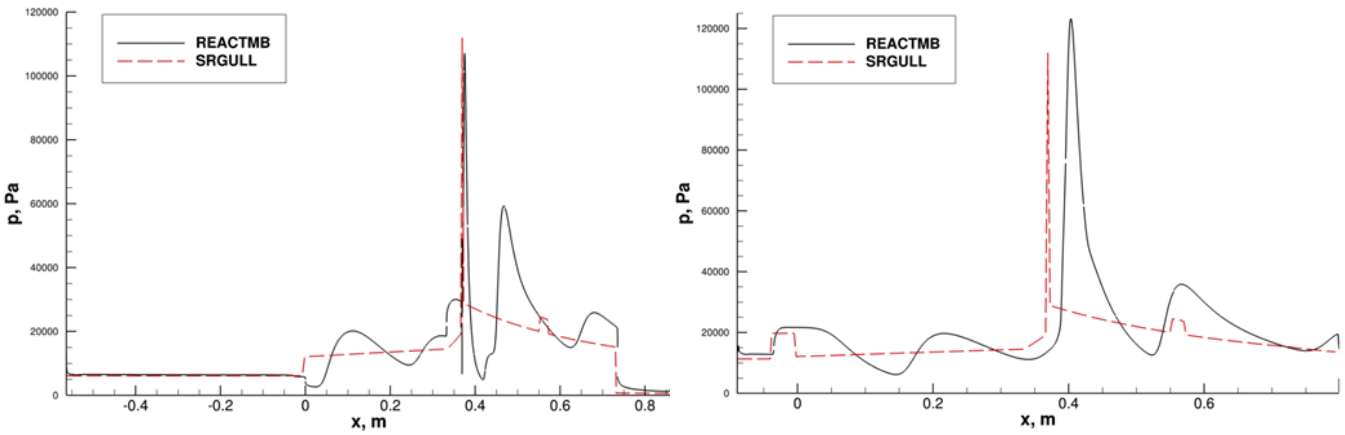

Figure 5: Body and cowl-side wall pressure distributions (mixing only case)

Similar results are presented in Table 2 and Figure 6 for the reactive case. Nose pitching moment agreement between the codes is improved, but normal force agreement is worse. The combustor exit flow is again predicted to be slightly faster by SRGULL, though the stream thrust at the exit (x-ST in the tables) is comparable. The injector is contributing ~90 percent of the overall thrust and the nozzle is producing next to none, indicating that the design chosen for this test case is not close to optimal.

Table 2: REACTMB/SRGULL Comparisons: Reacting

Cowl-To-Tail Data				
		REACTMB	SRGULL	% Error
Fx	N	-148.26	-145.3	2.0
Fy	N	-119.8	-105.4	12.0
Mz	N-m	-123.1	-120.8	1.9

Nose-To-Tail Data				
		REACTMB	SRGULL	% Error
Thrust	N	121.36	118.4	-2.4
Isp	s	134.6	131.3	-2.5

Inlet Throat Data				
		REACTMB	SRGULL	% Error
Mach		4.09	4.09	0.0
Static Press	Pa	12024	11955	-0.57
1D Vel (vdotn)	m/s	1911	1912	0.05
x-ST	N	278.8	279	0.07
y-ST	N	-16.04	-16.05	-0.31
Dynamic Pressure	Pa	138555	138127	-0.31
Static Temp	K	552	549	-0.54
Static Dens	kg/m^3	0.0756	0.0756	0.0
Mass Flow	kg/s	0.1398	0.1399	0.07

Combustor Exit Data				
		REACTMB	SRGULL	% Error
Mach		2.27	2.49	9.69
Static Press	Pa	30900	26407	-14.54
1D Vel (vdotn)	m/s	1580	1647	4.24
x-ST	N	420	427.9	1.88
y-ST	N	14.5	9.66	-33.38
Dynamic Pressure	Pa	105000	109402	4.19
Static Temp	K	1170	1034	-11.62
Static Dens	kg/m^3	0.0835	0.0808	-3.23
Mass Flow	kg/s	0.2309	0.2317	0.35

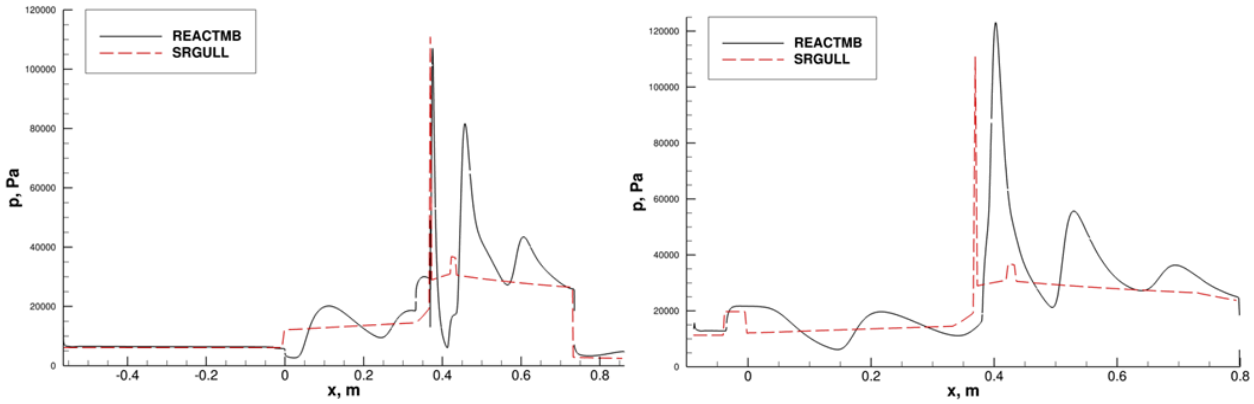

Figure 6: Body- and cowl-side wall pressure distributions (reacting case)

7.4. Bleed modeling

Results from the implementation of the Slater bleed model are discussed next. The test case is from Willis, et al. [29] and involves an oblique shock generated from an eight-degree wedge impinging on a turbulent boundary layer with a thickness of 2.63 cm. Bleed is induced through a plate drilled with 90 deg. circular holes with diameters of 0.635 cm. The porosity of the plate is 0.25. A plenum pressure of 5534 Pa is imposed, enabling a fully-choked state to be realized in all bleed ports. A 401×201 mesh is used for these 2D calculations. Figure 7 shows that that the use of boundary-layer bleed significantly reduces the level of flow separation as evidenced by the pressure plateau shown in the case without bleed. Agreement with the experimental pressure distribution is not very good, as the assumption of constant porosity prevents the flow from expanding and then re-compressing as it encounters individual bleed ports. The current predictions do compare well with Baurle and Norris's solutions with Slater's model [23], confirming the accuracy of the implementation.

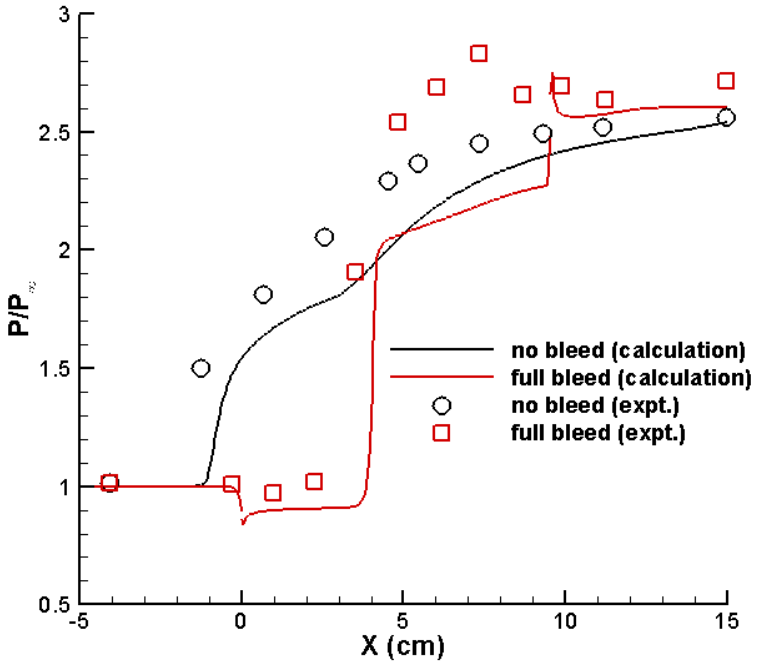

Figure 7: Wall pressure predictions with and without boundary-layer bleed (Willis, et al. experiments)

7.5. LES/RANS Simulations

The LES/RANS capabilities of REACTMB are highlighted in this section. The results presented are documented completely in [4, 5, 13, 20, 21]. All cases use the LES/RANS transition functions described in Section 3 in conjunction with either a 9-species hydrogen-air mechanism or a 22-species reduced ethylene-air mechanism. The cases shown correspond to experiments conducted at the University of Virginia's Scramjet Combustion Facility using three main configurations (termed Configurations C, E, and F). Configuration C injects hydrogen fuel behind a ramped wedge; Configuration E injects ethylene fuel through an array of small ports located upstream of a slanted cavity; and Configuration F injects fuel at the start of an isolator section. Configurations C and E can operate in 'scram-mode', with a shock train not present in the isolator, or in 'ram mode', in which a shock train is present in the isolator. Configuration F operates only in 'ram mode', as the shock train acts to mix fuel and air before it enters the combustor, enabling a pre-mixed flame front to be established. The simulations use between 60 and 100 M cells, with mesh sizes in the isotropic regions ranging between 0.2 and 0.35 mm. Experimental data available from the Scramjet Combustion Facility includes CARS, SPIV, wall pressure, TDLAS, OH-PLIF, and CH_2O-PLIF.

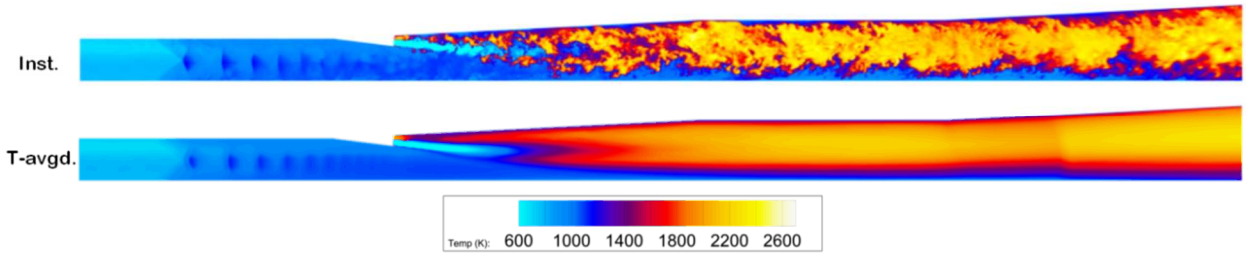

Figure 8: Instantaneous and averaged centerplane temperature distributions (Configuration C)

Figure 8 shows instantaneous and averaged centerplane temperature distributions for a Configuration C calculation that has transitioned to dual-mode operation. Figure 9 shows comparisons with CARS temperature measurements taken at different axial stations downstream of the ramped injector for a 'scram mode' case at an equivalence ratio of 0.17 The results show differences due to various subgrid-scale models for turbulence / chemistry interactions [21]. Figure 10 shows mean and *rms* wall pressure distributions compared with experimental data for this case.

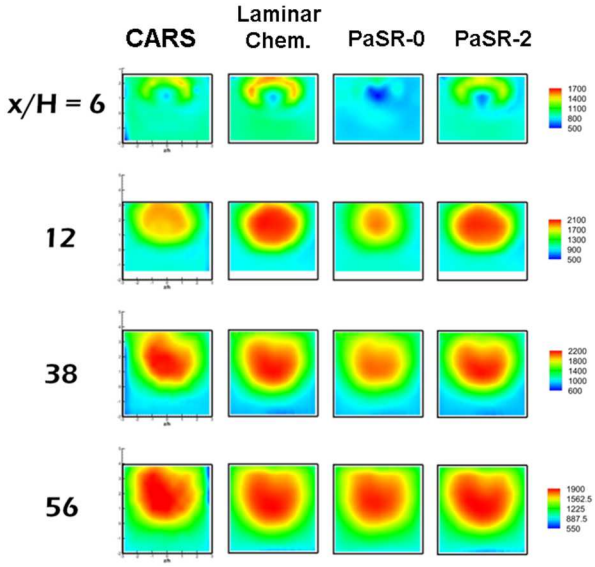

Figure 9: LES/RANS comparisons with CARS data (Configuration C)

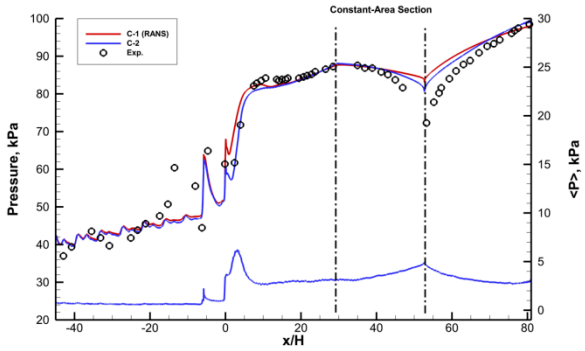

Figure 10: Wall pressure distributions

Results for Configuration E are shown in Figures 11-13. Figure 11 shows centerplane temperature predictions (top) along with a version of the Takeno flame index (bottom). The flame index shows that premixed combustion at fuel-rich conditions is characteristic of the

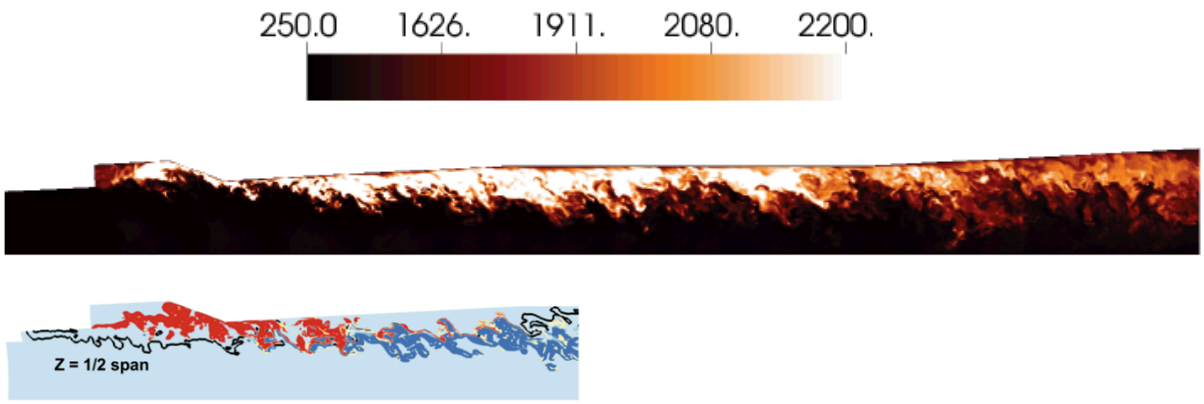

Figure 11: Centerplane temperature contours (top); Takeno flame index (bottom: red – rich premixed; blue – diffusion) – Configuration E ethylene / air combustion

cavity. As fuel is depleted, the flame structure transitions to a lean premixed flame and then to a diffusion flame.

Diagnostics for the Configuration E experiments are limited to wall pressure distributions and TDLAS line-of-sight predictions of temperature, CO, CO_2, and H_2O within and just downstream of the cavity. Figure 12 shows that the LES/RANS predictions agree very well with experimental wall pressure distributions. Cavity temperatures and CO_2 column densities are also predicted to good accord (Figure 13).

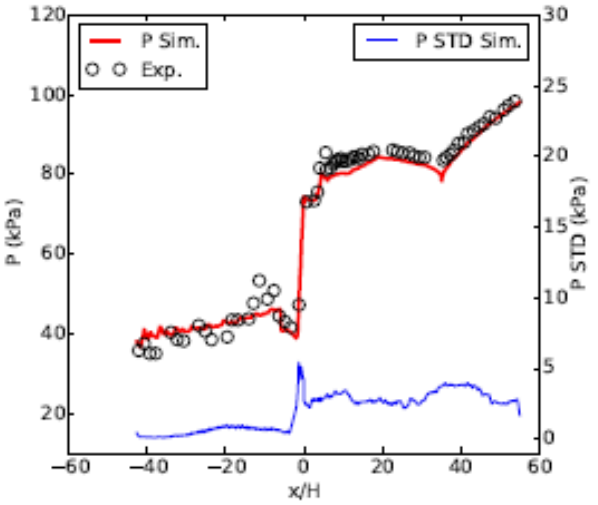

Figure 12: Wall pressure distributions (Configuration E)

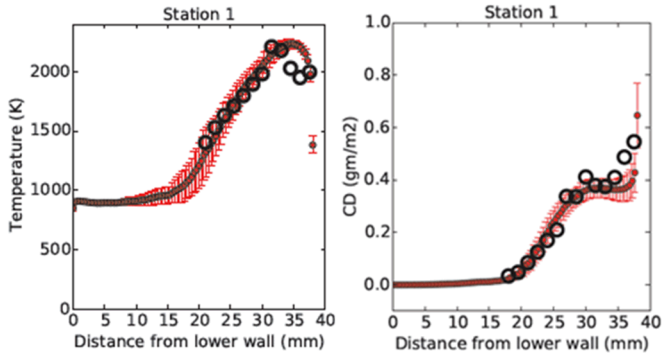

Figure 13: Comparisons with TDLAS line-of-sight profiles (left: temperature; Right: CO_2 column density)

Configuration F differs from the others in that it is designed to sustain premixed combustion in a high subsonic Mach number, high turbulence-intensity environment. As shown in Figure 13, a centerplane snapshot of ethylene mass fraction, mixing of fuel and air is initiated at the beginning of a long isolator and is enhanced significantly through interaction of the fuel plume with the isolator shock train. The equivalence ratio at the combustor entrance plane is ~0.4. A premixed combustion front is stabilized at the leading edge of the cavity and propagates across the combustor. Figure 14 provides a qualitative comparison of centerplane OH-PLIF data with

predicted OH mass fraction, while Figure 15 compares cavity-side wall pressure distributions with the computational prediction. The 'error bars' represent one standard deviation in pressure and show the level of large-scale unsteadiness predicted to occur in this system. The isolator shock train dynamics influences the local mixing process which in turns influences pre-mixed flame propagation, the formation of a thermal throat, and overall heat release, which feeds back to the shock train. The response is cyclic, with a predicted dominant frequency of 365 Hz. This value is in close agreement with time-resolved CH_2O imagery, which predicts a characteristic frequency of 325 Hz. .

Figure 13: Centerplane snapshot of ethylene mixing and combustion

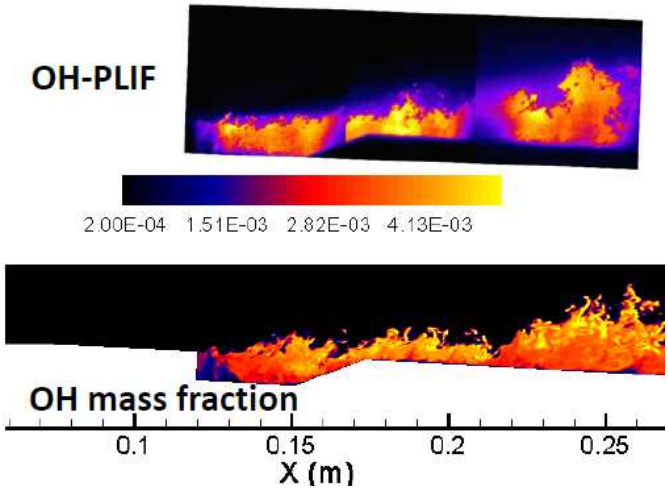

Figure 14: Centerplane OH-PLIF vs OH mass fraction

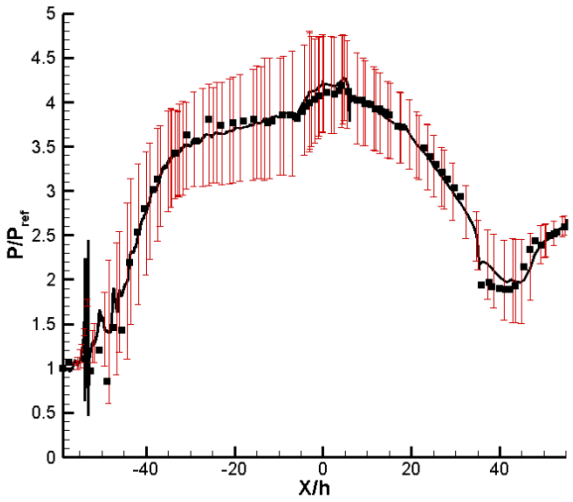

Figure 15: Centerplane wall pressure distribution

8. Conclusions

The development of a version of NCSU's REACTMB flow solver suitable for use in test and evaluation applications has been described. The code is capable of conducting large-scale 'tip-to-tail' simulations of high-speed engine flowpaths using RANS modeling and includes strategies for modeling bleed plates, methods for extracting performance measures, and simplified combustion models that provide the effects of bulk heat release on the engine response. REACTMB is also capable of detailed component studies using hybrid LES/RANS techniques and complex chemistry models. Several examples of the performance of REACTMB for both RANS and LES/RANS flow simulations have been shown. In general, good agreement with available experimental measurements has been obtained using both RANS and LES/RANS techniques, confirming the fidelity of the approach for flowpath and component simulations.

Acknowledgements

The development of REACTMB and its various sub-components has been supported by various ARO, AFOSR, NASA, and AFRL grants and contracts over the last ten years. Recent sources of support include AFOSR grants FA9550-09-1-0611 and FA9550-13-1-0049, focusing on LES/RANS simulations with detailed chemistry. The T&E version is supported by Sandia National Laboratories' Laboratory-Directed Research and Development Program. Computer resources have been provided by the NASA Advanced Supercomputing (NAS) division, NCSU's High Performance Computing facility, the DoD High Performance Computing Modernization Program, and the Department of Energy.

References

[1] Roy, C.J. and Edwards, J.R. "Numerical Simulation of a Three-Dimensional Flame / Shock Wave Interaction," *AIAA Journal*, Vol. 38, No. 5, 2000, pp. 745-760.
[2] Bond, R.B. and Edwards, J.R. "Computational Analysis of an Independent Ramjet Stream in a Combined Cycle Engine" *AIAA Journal*, Vol. 42, No. 11, 2004, pp. 2276-2284.
[3] Edwards, J.R., Boles, J.A., and Baurle, R.A. "Large-Eddy / Reynolds-Averaged Navier-Stokes Simulation of a Supersonic Reacting Wall Jet" *Combustion & Flame,* Vol. 159, No. 3, 2012, pp. 1127-1138.
[4] Fulton, J.A., Edwards, J.R., Hassan, H.A. , McDaniel, J.C., Goyne, C.P., Rockwell, R.D, Cutler, A.D., Johansen, C.T., and Danehy, P.M. "Large-Eddy / Reynolds-Averaged Navier-Stokes Simulations of Reactive Flow in a Dual-Mode Scramjet Combustor", *Journal of Propulsion and Power,* Vol. 30, 2014, pp. 558-575.
[5] Potturi, A.S. and Edwards, J.R. 'Large-Eddy / Reynolds-Averaged Navier-Stokes Simulation of Cavity-Stabilized Ethylene Combustion" *Combustion and Flame*, Vol. 162, No. 4, 2015, pp. 1176-1192.
[6] Edwards, J.R. "A Low-Diffusion Flux-Splitting Scheme for Navier-Stokes Calculations," *Computers Fluids*, Vol. 26, No. 6, 1997, pp. 635-659.
[7] Liou, M.-S. and Steffen, C.L. "A New Flux-Splitting Scheme" *Journal of Computational Physics*, Vol. 107, No. 1, 1993, pp. 23-39.
[8] Ducros, F., Ferrand, V., Nicaud, F., Weber, C., Darracq, D., Gachareiu, C., and Poinsot, T., "Large-Eddy Simulation of the Shock / Turbulence Interaction," *Journal of Computational Physics*, Vol. 152, No. 2, 1999, pp. 517–549.
[9] Menter, F. R., "Two-equation Eddy-viscosity Turbulence Models for Engineering Applications," *AIAA Journal*, Vol. 32, No. 8, 1994, pp. 1598-1605
[10] Gieseking, D.A., Choi, J.-I., Edwards, J.R., and Hassan, H.A. "Compressible Flow Simulations using a New LES/RANS Model" *AIAA Journal,* Vol. 49, No. 10, 2011, pp. 2194-2209.
[11] Lenormand, E., Sagaut, P., Ta Phuc, L, and Comte, P. "Subgrid-Scale Models for Large-Eddy Simulations of Compressible, Wall-Bounded Flows," *AIAA Journal*, Vol. 38, 2000, pp. 1340-1350.
[12] Salazar, G.. and Edwards, J.R. "Mach 6 Wake Flow Simulations using a Large-Eddy Simulation / Reynolds-Averaged Navier-Stokes Model", *Journal of Spacecraft and Rockets*, Vol. 51, pp. 1329-1348, 2014.

[13] Ramesh, K., Edwards, J.R., Goyne, C.P., McDaniel, J.C, Rockwell, B., Cutler, A.V., and Danehy, P. Large Eddy Simulation of High-Speed, Premixed Ethylene Combustion, AIAA 2015-0356, Jan. 2015.
[14] Burke, M. P., Chaos, M., Ju, Y., Dryer, F. L., and Klippenstein, S. J., "Comprehensive H2/O2 Kinetic Model for High-Pressure Combustion," *International Journal of Chemical Kinetics,* Vol. 44, No. 7, 2011, pp. 444–474.
[15] Jachimowski, C. J., "An Analysis of Combustion Studies in Shock / Expansion Tunnels and Reflected Shock Tunnels"," NASA TP-3224, 1992.
[16] Gokulakrishnan, P., Pal, S., Klassen, M., Hamer, A., Roby, R., Kozaka, O., and Menon, S., "Supersonic Combustion Simulation of Cavity-Stabilized Hydrocarbon Flames using Ethylene Reduced Kinetic Mechanism," AIAA Paper 2006-5092, 2006.
[17] Wang, T.-S., "Thermophysics Characterization of Kerosene Combustion", *Journal of Thermophysics and Heat Transfer,* Voll. 15, No. 2, pp. 140-147, 2001.
[18] Luo, Z., Yoo, C. S., Richardson, E. S., Chen, J. H., Law, C. K., and Lu, T., "Chemical Explosive Mode Analysis for a Turbulent Lifted Ethylene Jet Flame in Highly-Heated Coflow," *Combustion and Flame*, Vol. 159, No. 1, 2012, pp. 265–274.
[19] Magnussen, B. F., "The Eddy Dissipation Concept for Turbulent Combustion Modeling. Its Physical and Practical Implications," Report N-7034, Division of Thermodynamics, Norwegian Institute of Technology, Trondheim, Norway, 1989.
[20] Potturi, A and Edwards, J.R. "Investigation of Subgrid Closure Models for Finite-Rate Scramjet Combustion", AIAA Paper 2013-2461, 2013
[21] Fulton, J.A., Edwards, J.R., Cutler, A.D., McDaniel, J.C., Goyne, C.P. "Turbulence / Chemistry Interactions in a Ramp-Stabilized Supersonic Hydrogen-Air Diffusion Flame" AIAA 2014-0627, 2014.
[22] Ghosh, S., Choi, J.-I., and Edwards, J.R. "Simulation of Shock Boundary Layer Interactions with Bleed using Immersed Boundary Methods" *Journal of Propulsion and Power*, Vol. 26, No. 2, 2010.
[23] Baurle, R.A. and Norris, A.T. "A Source Term Based Boundary Layer Bleed / Effusion Model for Passive Shock Control" JANNAF, 2012.
[24] Slater, J.W., "Improvements in Modeling 90-degree Bleed Holes for Supersonic Inlets", AIAA Paper 2009-0710 (Jan. 2009).
[25] Baurle, R.A. and Gaffney. R.J., "Extraction of One-dimensional Flow Properties from Multidimensional Data Sets" *Journal of Propulsion and Power*, 24(4):704–714, 2008
[26] Vogel, P.D. and Edwards, J.R. "Numerical Simulation of a Hypervelocity Scramjet Engine Using Silane – Hydrogen Fuel", AIAA Paper 2012-3773.
[27] Milligan, R. T., Liu, J., Tam, C.-J., Eklund, D. R., Hagenmaier, M. A., Davis, D. L., Risha, D. J., Gruber, M., and Mathur, T. "Dual-Mode Scramjet Combustor: Numerical Sensitivity and Evaluation of Experiments." AIAA Paper 2012-0947.
[28] Pinckney, S. Z., Ferlemann, S. M., Mills, G., and Takashima, N. "Program Manual for SRGULL Ver. 1.0: Second Generation Engineering Model for the Prediction of Airframe-Integrated Subsonic/Supersonic Combustion Ramjet Cycle Performance." Hyper-X 829, July 2000.
[29] Willis, B. P., Davis, D. O., and Hingst, W. R., "Flowfield Measurements in a Normal-Hole-Bled Oblique Shock-Wave and Turbulent Boundary-Layer Interaction", AIAA Paper 1995-2885 (July 1995).